applied optics

Intensity enhancement in off-axis integrated cavity output spectroscopy

Faisal Nadeem,* Julien Mandon, Simona M. Cristescu, and Frans J. M. Harren

Trace Gas Research Group, Molecular and Laser Physics, Institute for Molecules and Materials, Radboud University, Nijmegen, The Netherlands
**Corresponding author: f.nadeem@science.ru.nl*

Received 28 June 2018; revised 6 September 2018; accepted 7 September 2018; posted 10 September 2018 (Doc. ID 336439); published 2 October 2018

In the field of laser-based absorption spectroscopy, off-axis integrated cavity output spectroscopy is considered to be a sensitive and robust method, employing a simple optical design. However, one of the major drawbacks of non-mode-matched cavities combined with highly reflective mirrors (>99.98%) is its low output intensity. Here, we systematically investigate the increase in cavity output intensity, using a third re-injection mirror before the absorption cavity. The presented design not only enables high transmission power but also retains a long effective path length. To investigate the intensity enhancement, we used a CO_2 absorption line in the near-IR wavelength region at 6240.10 cm^{-1}. In agreement with our simulation model, we achieved an intensity enhancement factor of 38. We achieved a noise equivalent absorption sensitivity to 1.6×10^{-8} cm^{-1} $Hz^{-1/2}$, which is no longer limited by the detectivity of the detector.

OCIS codes: (140.4780) Optical resonators; (300.1030) Absorption; (300.6360) Spectroscopy, laser.

https://doi.org/10.1364/AO.57.008536

1. INTRODUCTION

Laser-based absorption spectroscopy is well suited for trace gas analysis, because of its ability to provide a high degree of sensitivity and selectivity; it quantifies trace gas mixtures both accurately and quickly, down to parts-per-billion volume (ppbv, $1:10^9$) and even parts-per-trillion volume (pptv, $1:10^{12}$) mixing levels [1]. Such ultrasensitive measurements are of increasing interest for applications such as in biomedical human breath analysis [2–5] and environmental monitoring [6,7]. A high sensitivity is achieved by long absorption path lengths, which can be obtained by using multipass cells, such as White [8], Herriott, and Schulte [9], or astigmatic cells [10] up to few hundred meters. Alternatively, to reach path lengths in kilometers, cavity enhanced methods are the preferred platform [7,11–13]. Methods such as cavity ring-down spectroscopy (CRDS) [14], integrated cavity output spectroscopy (ICOS) [15,16], or noise immune cavity enhanced optical heterodyne molecular spectroscopy (NICE-OHMS) [12] not only provide opportunities for the laser light to interact with the gas over longer path lengths, but also can handle the laser intensity/frequency fluctuations [17]. While CRDS and NICE-OHMS require active feedback control of the optical cavity, off-axis (OA)-ICOS can passively couple laser light into an optical cavity. This makes it less demanding, simple, and robust with sensitivities comparable to CRDS [18]. With its simplicity and no need to lock the cavity to the laser, OA-ICOS is a very promising for field applications.

When laser light is coupled through the center of an optical cavity, the transmission frequencies of the light are separated by the large free spectral range (FSR) of the cavity (FSR $= c/2L$, with L as length cavity, c as the speed of light). For high-finesse cavities (e.g., $F \sim 15{,}000$), the cavity mode linewidths are in the low kilohertz (kHz) range. Using laser linewidths in the kHz–MHz (megahertz) range, the laser transmission through the high-finesse cavity will result in optical intensity fluctuations [15,18–20]. This can be avoided by locking the laser fully to the optical cavity, such as that proposed in NICE-OHMS [12] and CRDS [14]. Alternatively, continuous-wave (CW) CRDS can be performed by sweeping the optical cavity length or the laser frequency over one FSR of the cavity. However, in that case, the laser transmission time will be very short (in the order of microseconds). By locking the laser to the optical cavity, the interaction time will be 100%, resulting in a high data acquisition rate, improving the signal to noise ratio (SNR) [21].

When the laser light is coupled in an OA configuration, it makes multiple roundtrips in the cavity ($s = 2mL$, where s is the laser path length, L is the cavity length, and m is the number of roundtrips) instead of one roundtrip ($s = 2L$) before it returns to its point where it enters the cavity. This reduces the FSR of the cavity by a factor of m. With this reduced FSR, more cavity modes will be underneath the laser linewidth, which smooths the laser transmission intensity. As a result, the intensity noise will be strongly reduced [1,18,22,23]. OA-ICOS not only avoids the need for controlling the absorption cavity, but

also eliminates the need of acoustic–optic modulators and piezoelectric transducers [24]. Furthermore, OA-ICOS is relatively less sensitive to misalignment and also overcomes optical feedback from the cavity mirror into the laser.

For a mode-matched (on-axis) and impedance-matched high-finesse cavity, a large fraction of the original laser power can be coupled out. In the OA configuration, the optical cavity is non-mode-matched and combined with highly reflective mirrors (e.g., 99.98% reflectivity), so the transmitted intensity will be only a small fraction (here 0.01%) of the original intensity; the rest will be reflected backward and lost [22,25,26]. This affects the performance of OA-ICOS. In addition, for the mid-IR wavelength region, detectors have typically 1–3 orders of magnitude lower detectivity (D*) compared to near-IR detectors (see, e.g., [27]). As a result, it is difficult to achieve high absorption sensitivity using high-finesse optical cavities with highly reflective mirrors due to the low throughput intensity. As such, higher laser intensities are needed in the mid-IR wavelength, not to be limited by the detector noise.

To couple more light into the optical absorption cavity, we placed an additional third mirror (re-injection mirror) in front of the first cavity mirror to re-inject the back-reflected light from the first cavity mirror into the absorption cavity. Initially, the laser light enters through a small entrance hole in the re-injection mirror (see Fig. 1). Previously, an intensity enhancement factor of 22.5 was achieved by O'Keefe and Leen [28]. Centeno *et al.* have shown four-fold and ten-fold (transmission intensity enhancement factor of 28) improvements in sensitivity in comparison with standard OA-ICOS using a pulsed quantum cascade laser working at 915 cm^{-1} (wavelength 10.9 μm) [25,29].

Recently, we developed a comprehensive three-dimensional ray tracing model to simulate optical re-injection using OA-ICOS [30]. We maximized the optical intensity throughput and absorption path length via a grid search and genetic algorithm. With this model, intensity enhancement factors up to 1400 could be found for short (3-cm-long) cavities and up to 101 for long (50 cm) cavities. In this paper, we experimentally verify this three-dimensional ray tracing model using a 30-cm-long absorption cavity. In addition, we used larger diameter re-injection mirrors to maximize the re-injection effect [30]. To demonstrate its usefulness for spectroscopy, we used a CO_2 absorption line in the near-IR wavelength region at 6240.10 cm^{-1}. Furthermore, we investigated the effect of high and low laser intensities on the detection sensitivity.

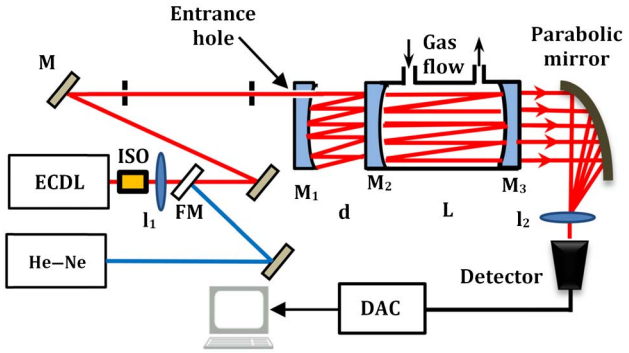

Fig. 1. Overview of the CW ECDL in combination with three-mirror OA-ICOS set-up. The beam enters the cavity via a lens (l_1) and an entrance hole in the re-injection mirror M_1. The absorption cavity is provided with a gas in- and outlet. He–Ne, helium-neon Laser; ECDL, external cavity diode laser; $M_{2,3}$, cavity mirrors; ISO, optical isolator; L and d, absorption and re-injection cavity lengths, respectively; FM, flip mirror; DAC, data acquisition card.

2. EXPERIMENTAL SETUP

For the verification and validation of our developed three-dimensional ray tracing model, we combined a CW external cavity diode laser (ECDL, DL Pro, Toptica, 50 mW) tunable from 1510 to 1630 nm (6135–6623 cm^{-1}) with a high-finesse optical cavity and re-injection mirror. The laser has a linewidth of 60 kHz (in 5 μs). The laser light passed through an optical isolator (ISO, IO-4-1650 VLP, Thor Labs) providing 30 dB isolation. The aluminum gas absorption cell ($L = 30$ cm) has spherical mirrors [$\varnothing = 2.54$ cm, radius of curvature (ROC), $M_{2,3} = 100$ cm, $r \sim 99.50\%$ at 1650 nm, and AOI = 0°, Layertec, Germany], providing an optical finesse of ~626 and an effective path length of 60 m.

The re-injection mirror M_1 has a distance d to mirror M_2. A mode matching lens (l_1, ZnSe, $f = 100$ cm) is utilized to focus the light into the center of the absorption cavity (beam waist 0.5 mm).

To investigate the optical re-injection effect, we deployed two types of re-injection mirrors (M_1): a metallic gold-coated mirror [$\varnothing = 50.8$ mm, (5.08 cm mirror), ROC = 100 cm, $r \sim 96\%$, Thor Labs, Germany] and a concave dielectric-coated IR mirror [$\varnothing = 76.2$ mm (7.62 cm mirror), ROC = 100 cm, $r \sim 99\%$, Thor Labs]. In both mirrors, a small entrance hole was drilled ($\varnothing = 1$ mm) at 10 mm from the center of the curvature.

A visible He–Ne laser is used to facilitate the alignment of the IR beam into the optical cavities. Coarse tuning of the ECDL is performed via a piezo actuator (PZT), controlling the grating angle. The transmitted light is collected with a parabolic mirror ($f = 20$ cm) and is focused via a lens (l_2, BaF_2, $f = 25$ mm) onto a fast photodetector (LCA-S-400K-IN, Femto Messtechnik, Germany). The photodetector signal is analyzed via a data acquisition card (DAC, GaGe Octopus-8325, 14 bit, USA) and a LabVIEW program. A Fourier transform IR spectrometer (Nicolet Magna 560, France, spectral resolution 0.125 cm^{-1}) is used to monitor the wavelength of the laser.

For optimal alignment, the laser beam is first aligned on-axis with the absorption cavity, using a mode matching lens (l_1). Second, CO_2 gas is introduced in the absorption cell via a gas flow system, and a single CO_2 absorption line is detected at 6240.10 cm^{-1}. In the third step, the transmission properties of the cavity are changed by going to the OA configuration (~10 mm OA from the center of the curvature of the mirrors), thereby optimizing the SNR of the CO_2 absorption line. This has been achieved by translating the mirrors perpendicular to the laser beam, inducing a circular/elliptical spot pattern (from the He–Ne laser) [31] at the mirror surfaces, thereby reducing the intensity noise level at the baseline of the CO_2 line. In the fourth step, the re-injection mirror is placed, the light is coupled through the entrance hole, and the system is optimized again for maximum SNR on the detector.

Inside the absorption cell, a constant gas flow is maintained at a 200 mbar pressure by adjusting two needle valves in the tubing before and after the cell and using a vacuum pump. For the volume mixing ratio of CO_2 in nitrogen, two mass flow controllers (Brooks Instruments, USA) are used. The PZT is swept by a 15 Hz saw tooth waveform. A single absorption line of the CO_2 is scanned in 60 ms. Furthermore, the data is acquired at a sampling rate of 1 kS/s and is averaged over ten scans in 0.6 s.

3. RESULTS AND DISCUSSIONS

Figures 2(a) and 2(b) show the measured data for the CO_2 absorption line with and without the re-injection mirror. By placing a re-injection mirror M_1 with a small entrance hole at a distance d from the first absorption cavity mirror M_2, an intensity enhancement of the laser power is achieved. In both of the panels, the distance d is normalized to the ROC of the re-injection mirror R, i.e., d/R. We used a 7.62 cm and a 5.08 cm diameter mirror for panels (a) and (b) in Fig. 2, respectively. As can be seen both, the laser intensity enhancement and the CO_2 absorption line depth depend upon the d/R ratio. The total amount of light on the detector is enhanced using the re-injection mirror: the background and absorption line intensity are multiplied with the same value.

The intensity enhancement (P_{enhanced}) for the total power can be calculated using the model [30]

$$P_{\text{enhanced}} = \frac{I_{3\text{–mirror}}}{I_{2\text{–mirror}}} = \frac{\sum_{i=0}^{n} r^{2i} m_i}{m_0}, \tag{1}$$

where $I_{3\text{–mirror}}$ and $I_{2\text{–mirror}}$ are the intensities with and without the re-injection mirror, r is the mirror reflectivity, n is the number of roundtrips in the re-injection cavity, m_i is the number of roundtrips in the absorption cavity from spot i on M_2, and m_0 is the number of roundtrips with $i = 0$ (no re-injection mirror).

We measured the intensity enhancement as a ratio of the intensity with the re-injection mirror to that without a re-injection mirror while monitoring a single CO_2 absorption line. The intensity enhancement factors were measured at seven d/R points by placing the re-injection mirror (M_1) and ultimately changing the distance of the re-injection mirror to the absorption cavity front mirror (M_2). Afterward, we simulated the enhancement factors in both configuration cases by inputting the experimental cavity parameters such as reflectivity, diameters, and ROC of the mirrors in the developed three-dimensional ray tracing model.

A comparison of intensity enhancement factors, between the measured and modeled data at different d/R ratios, is shown in Fig. 3. We observed a good agreement between the theory and the experiment. Maximum measured enhancement factors are found of 16 and 38 for the 5.08 cm ($r \sim 96\%$) and 7.62 cm re-injection mirrors ($r \sim 99\%$), respectively. At low d/R values the experimental results are lower than the simulated data. We believe that this is originating from the use of our three-dimensional ray tracing model and not using a Gaussian beam profile for the optical beam. At shorter distances d, the entrance hole becomes of relatively more import, and the Gaussian beams will clip at the entrance hole.

To accurately calculate the integrated area of the CO_2 absorption line for each d/R ratio, we used the Voigt profile of 2.6% CO_2 in N_2 (HITRAN 2012 database [32], pressure 200 mbar, room temperature, 60 m effective path length). The integrated area under the curve and the determined error are shown in Fig. 4. The full width at half-maximum of the measured lines was 0.030 cm^{-1} (900 MHz).

The higher enhancement factor for the 7.62 cm mirror is solely due to its higher reflectivity. To see whether an increased diameter of the re-injection mirror can change the intensity enhancement factor, we modeled the enhancement factor for three sets of the re-injection mirror diameters, as shown in Fig. 5, as a function of the re-injection mirror reflectivity, while keeping the mirror reflectivity of the absorption cavity constant. A substantial change in the enhancement factor can be seen with increasing re-injection mirror diameters from 2.54 cm to 5.08 cm. However, the increase is negligible while going from 5.08 cm to 7.62 cm.

From Fig. 3, it is obvious that there is a minimum enhancement factor at $d/R = 0.5$, while there is a maximum

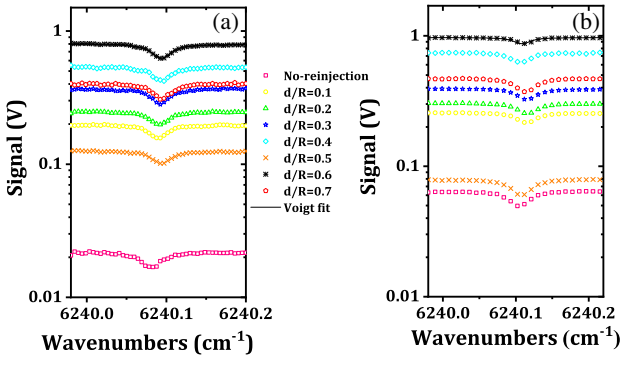

Fig. 2. Measured signal (every 20th point is shown, 10 scans average) of the CO_2 absorption line at 6240.10 cm^{-1} for a 2.6% mixture of CO_2 in N_2 without and with the re-injecting mirror at various d/R ratios. (a) 7.62 cm re-injection mirror (99% reflectivity), (b) 5.08 cm re-injection mirror (96% reflectivity). The zero intensity levels in both panels are at 0 V.

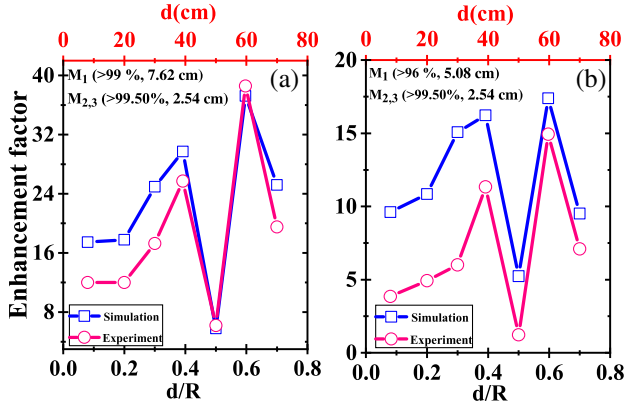

Fig. 3. Comparison of simulations by the three-dimensional ray tracing model and measured experimental data. Intensity enhancement factors at various d/R ratios are shown in Figs. 2(a) and 2(b). Blue line, simulation; magenta line, experimental data. (a) 7.62 cm re-injection mirror, (b) 5.08 cm re-injection mirror.

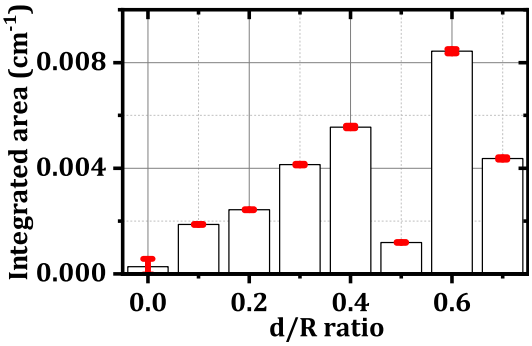

Fig. 4. Integrated area of the CO_2 absorption profile as a function of the d/R ratio (7.62 cm re-injection mirror) for 2.6% CO_2 in N_2 at 200 mbar pressure with the effective path length of 60 m. Note that $d/R = 0$ corresponds to no re-injection.

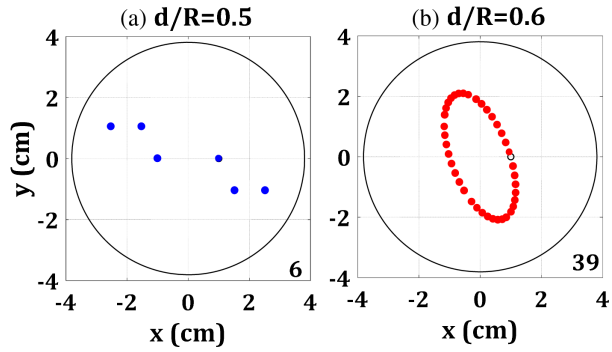

Fig. 6. Simulated spot patterns on the surface of the 7.62 cm re-injection mirror (ROC = 100 cm, $r \sim 99\%$), entrance hole 1 mm) for two re-injection cavity lengths. (a) $d/R = 0.5$, (b) $d/R = 0.6$ in combination with 2.54 cm absorption cavity mirrors at optimized beam entrance angles (ROC = 100 cm, OA distance entrance hole is 10 mm).

enhancement factor at $d/R = 0.6$ for both configurations. To clarify this, we simulated the spot pattern with our model at the surface of the re-injection mirror for Fig. 3(a). The laser beam exits the re-injection cavity already after six roundtrips through the entrance hole, irrespective of its initial entrance angles and positions at $d/R = 0.5$ (see Fig. 6). This might be due to the fact that distance between the re-injection mirror and the first absorption cavity mirror is equivalent to the focal length of the re-injection mirror [30]. At $d/R = 0.6$, an ellipse consisting of 39 roundtrips (laser beam entrance angles $\alpha_x = -0.4°$, $\alpha_y = -0.6°$ in the x, y direction) is found, which corresponds to a maximum enhancement factor of 38. These observations are in agreement with Eq. (1), indicating that the enhancement factor is almost proportional to the number of roundtrips in the injection cavity.

In order to properly characterize the system performance with and with without the re-injection mirror, we performed measurements in two cases. In the first test, we recorded the laser power signal (in volts) over a spectral span with only nitrogen gas in the absorption cell). To observe an enhancement in intensity and SNR at low power, we reduced the power of the laser with an optical attenuator down to $P = 75$ μW so that signal onto the detector is slightly above the noise level of the detector. Figure 7(a) shows the absolute signals, and Fig. 7(b) shows the Allan deviation plots in the SNR of the detector (black curve, average amplitude 1 mV), no re-injection mirror (blue curve, average amplitude 13 mV), and with the re-injection mirror at $d/R = 0.6$ (red curve, amplitude 500 mV).

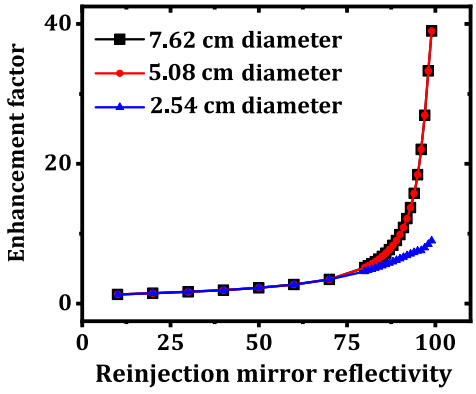

Fig. 5. Modeled enhancement factor as a function of the re-injection mirror diameter and reflectivity ($d/R = 0.6$, ROC = 100 cm, $d = 60$ cm), absorption cavity parameters ($L = 30$ cm, $M_{2,3} = 2.54$ cm, ROC = 100 cm, $r = 99.5\%$). Note that in these simulations the symmetric mirrors with equal ROCs are used.

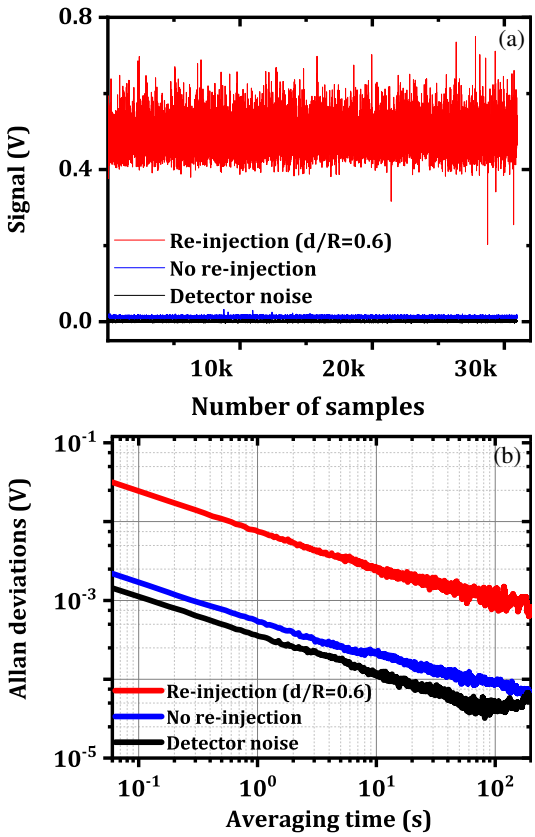

Fig. 7. Allan deviation plots using low laser power (75 μW) of SNR of the detector (black curve), SNR of the laser intensity without the re-injection mirror (blue curve), and after placing the re-injection mirror at $d/R = 0.6$ (red curve). The absorption cell contained pure N_2 gas.

An intensity enhancement factor of 38 (absolute DC signal) was obtained. This resulted in a 16-fold increase in SNR, as compared to using no re-injection mirror. The lower enhancement in SNR is due to intensity noise added by transmission through the ICOS cavity. The test allows us to evaluate absolute values of the intensity and the SNR without the influence of absorption measurements.

In the second test, we evaluated the long-term stability, detection limits, precision, and sensitivity for molecular spectroscopy by applying concentration mixtures. For this, we continuously scanned the laser across the CO_2 absorption line using a calibrated CO_2 mixture in N_2. We compared the measured absorption line with a reference scan in a linear way (see Fig. 8) using the $d/R = 0.6$ configuration. Here, this is with the same method under the same conditions; in general, the reference scan can be made with a calibrated gas mixture. Each time (frequency) point of the absorption line is compared to the same frequency point of the reference sample in the x, y coordinates [Fig. 8(b)]. The slope of the fit determines the relative concentration change; the uncertainty in the slope defines the uncertainty in the concentration.

The advantage of this approach is that the data points, which are in close proximity to the line center, mostly determine the slope of the fit (and its uncertainty). Another advantage is the fast determination of the concentration, with no need for fitting the absorption line to a lineshape. Furthermore, any concentration can be determined as long as there is a reference line shape from a gas sample. This procedure can also be used for line multiplets, congested lines, or complete vibrational bands and have been successfully applied previously [29,33,34].

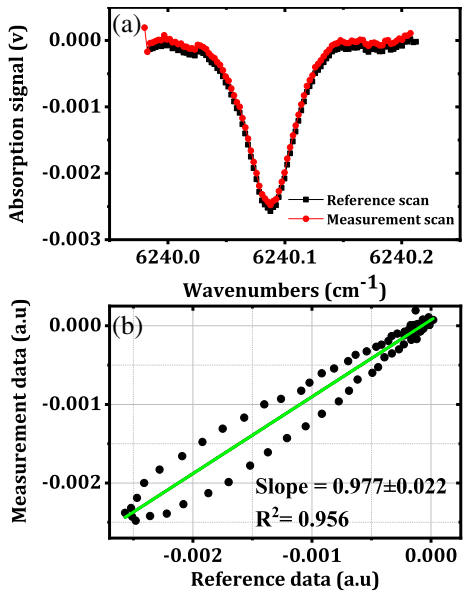

Fig. 8. Data acquisition procedure. (a) Measured background subtracted absorption lines without the re-injection mirror (400 ppmv CO_2 in N_2, pressure 200 mbar, path length 60 m, scan time 60 ms, 10 averages, background level ~0.02 V). (b) Scatter plot of the measured data against the reference data and corresponding linear fit.

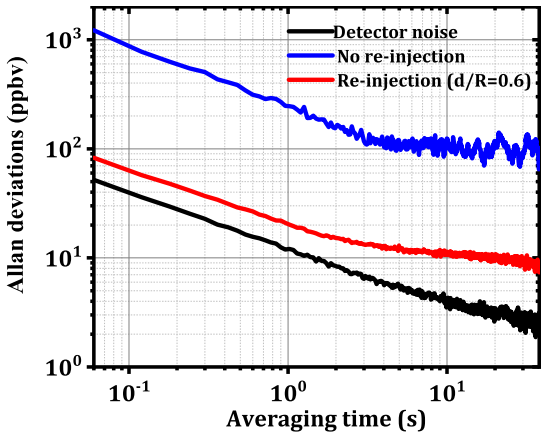

Fig. 9. Allan deviation as a function of averaging time for 10 ppmv of CO_2 in N_2 without (blue line) and with (red line) the re-injection mirror. A factor of 14.5 sensitivity enhancement was achieved using the re-injection mirror. The black line is the sensitivity for the dark current of the detector. A MDA of 10 ppbv in 10 s is achieved using the re-injection mirror.

Using the data acquisition procedure shown in Fig. 8, we evaluated the sensitivity of the three-mirror system at the low laser intensity (~75 μW). At high laser intensities, laser intensity fluctuations will be limiting, while at low laser intensity the detectivity of the detector is the limiting factor. In the latter case, the use of a re-injection mirror is feasible. We measured the absorption depth of a 10 ppmv of CO_2 in N_2, with and without the 7.62 cm re-injection mirror at $d/R = 0.6$. After each scan, we retrieved the concentration by comparing this scan to the reference gas by fitting a first-order polynomial [slope value, Fig. 8(b)]. With a slope value of one, the unknown concentration is equivalent to the reference gas concentration. The retrieved concentration is recorded over time, and an Allan deviation plot was made (Fig. 9), from which the minimum detectable absorption (MDA) was calculated.

A MDA of less than 10 ppbv of CO_2 in N_2 in 10 s averaging time is achieved using the re-injection mirror, which is a factor of 14.5 better than using it without the re-injection mirror. The noise equivalent absorption sensitivity (NEAS) can be calculated according to [18]

$$\mathrm{NEAS} = \left(\frac{\Delta I}{I}\right)\frac{1}{L_{\mathrm{eff}}}\sqrt{\frac{nT}{N_p}}, \tag{2}$$

in which T is the acquisition time (here, 0.06 s), L_{eff} is the effective path length ($L_{\mathrm{eff}} = 60$ m), n is the number of the scans averaged (10 in 1 s), and N_p is the number of points per scan (100). As such, we achieved a NEAS of 1.6×10^{-8} $\mathrm{cm^{-1}\,Hz^{-1/2}}$ with the re-injection mirror.

For maximum laser intensity onto the detector, several extra points have to be taken into account. Lenses with long focal lengths in front of the cavity are required to avoid clipping of the laser light at the entrance hole of the re-injection mirror. Furthermore, the re-injection mirror diameter should be substantially larger than the cavity mirror diameter to effectively re-inject all of the reflected light (also at larger beam angles).

Behind the optical cavity, it is difficult to collect all of the light onto a single point detector, even with the use of a parabolic mirror, as the light rays at the output of the cavity are inherently skewed and divergent from the optical axis. The latter can be improved with the use of the lenses, however, skewness is difficult to tackle and often leads to an insufficient collection of the light [35]. Consequently, a trade-off between the active area of the detector and cavity mirror diameter should be made.

4. CONCLUSIONS

Here, we systematically investigated the increase in cavity output intensity, using a re-injection mirror before the absorption cavity. The present design not only enables high transmission intensity but also retains a long effective path length. To investigate the intensity enhancement, we used a single CO_2 absorption line at 6240.10 cm^{-1}. In agreement with our model calculations, we achieved a maximum intensity enhancement factor of 38 (using a 7.62 cm re-injection mirror with 99% reflectivity).

Non-mode-matched optical cavities with high-reflectivity mirrors have a low-intensity output. If detectors with a low detectivity are used, detector noise becomes a dominant factor instead of laser intensity noise. The latter is particularly interesting for the mid- and far-IR wavelength regions with low-detectivity detectors [27]. The re-injection mirror increased the transmission intensity and improved the SNR and subsequently the NEAS.

Thanks to the demonstration of this method, one can use of the detectors that are not particularly sensitive, especially in the mid-IR. High-sensitivity detectors are only available at low (liquid nitrogen) temperatures. Furthermore, it is important to have short absorption cavities with a small footprint in a small overall sensor design. To have the same effective path length for a short absorption cavity as for a long absorption cavity, higher mirror reflectivities are needed. However, this results in a low intensity to the detector. By using a re-injection mirror, the output intensity can be increased above the noise floor of the detector. From our model, it is shown that improved enhancements can be achieved by using shorter cavities with larger diameters [30]. This will trigger new opportunities in the field of ultrasensitive gas detection using compact optical gas sensors with a small footprint.

Funding. Seventh Framework Programme (FP7) (286409).

Acknowledgment. This research work is supported by the European project QUANTATEC in the FP7-Framework Programme: Marie Curie Actions-Industrial-Academia Partnerships and Pathways (IAPP).

REFERENCES

1. D. D. Arslanov, S. M. Cristescu, and F. J. M. Harren, "Optical parametric oscillator based off-axis integrated cavity output spectroscopy for rapid chemical sensing," Opt. Lett. **35**, 3300–3302 (2010).
2. D. D. Arslanov, K. Swinkels, S. M. Cristescu, and F. J. M. Harren, "Real-time, subsecond, multicomponent breath analysis by optical parametric oscillator based off-axis integrated cavity output spectroscopy," Opt. Express **19**, 24078–24089 (2011).
3. B. Tuzson, J. Jágerská, H. Looser, M. Graf, F. Felder, M. Fill, L. Tappy, and L. Emmenegger, "Highly selective volatile organic compounds breath analysis using a broadly-tunable vertical-external-cavity surface-emitting laser," Anal. Chem. **89**, 6377–6383 (2017).
4. C. Wang and P. Sahay, "Breath analysis using laser spectroscopic techniques: breath biomarkers, spectral fingerprints, and detection limits," Sensors **9**, 8230–8262 (2009).
5. M. Gianella and G. A. D. Ritchie, "Cavity-enhanced near-infrared laser absorption spectrometer for the measurement of acetonitrile in breath," Anal. Chem. **87**, 6881–6889 (2015).
6. A. Kosterev, G. Wysocki, Y. Bakhirkin, S. So, R. Lewicki, M. Fraser, F. Tittel, and R. F. Curl, "Application of quantum cascade lasers to trace gas analysis," Appl. Phys. B **90**, 165–176 (2008).
7. J. Hodgkinson and R. P. Tatam, "Optical gas sensing: a review," Meas. Sci. Technol. **24**, 012004 (2013).
8. J. U. White, "Long optical paths of large aperture," J. Opt. Soc. Am. **32**, 285–288 (1942).
9. D. R. Herriott and H. J. Schulte, "Folded optical delay lines," Appl. Opt. **4**, 883–889 (1965).
10. J. B. McManus, P. L. Kebabian, and M. S. Zahniser, "Astigmatic mirror multipass absorption cells for long-path-length spectroscopy," Appl. Opt. **34**, 3336–3348 (1995).
11. G. Berden, R. Peeters, and G. Meijer, "Cavity ring-down spectroscopy: experimental schemes and applications," Int. Rev. Phys. Chem. **19**, 565–607 (2000).
12. J. Ye, L.-S. Ma, and J. L. Hall, "Ultrasensitive detections in atomic and molecular physics: demonstration in molecular overtone spectroscopy," J. Opt. Soc. Am. B **15**, 6–15 (1998).
13. A. O'Keefe, "Integrated cavity output analysis of ultra-weak absorption," Chem. Phys. Lett. **293**, 331–336 (1998).
14. A. Okeefe and D. A. G. Deacon, "Cavity ring-down optical spectrometer for absorption measurements using pulsed laser sources," Rev. Sci. Instrum. **59**, 2544–2551 (1988).
15. R. Engeln, G. Berden, R. Peeters, and G. Meijer, "Cavity enhanced absorption and cavity enhanced magnetic rotation spectroscopy," Rev. Sci. Instrum. **69**, 3763–3769 (1998).
16. A. O'Keefe, J. J. Scherer, and J. B. Paul, "CW integrated cavity output spectroscopy," Chem. Phys. Lett. **307**, 343–349 (1999).
17. H.-P. Loock and G. Gagliardi, *Cavity-Enhanced Spectroscopy and Sensing* (Springer, 2014).
18. E. J. Moyer, D. S. Sayres, G. S. Engel, J. M. S. Clair, F. N. Keutsch, N. T. Allen, J. H. Kroll, and J. G. Anderson, "Design considerations in high-sensitivity off-axis integrated cavity output spectroscopy," Appl. Phys. B **92**, 467–474 (2008).
19. G. Meijer, M. G. H. Boogaarts, R. T. Jongma, D. H. Parker, and A. M. Wodtke, "Coherent cavity ring down spectroscopy," Chem. Phys. Lett. **217**, 112–116 (1994).
20. J. Courtois, A. K. Mohamed, and D. Romanini, "High-speed off-axis cavity ring-down spectroscopy with a re-entrant configuration for spectral resolution enhancement," Opt. Express **18**, 4845–4858 (2010).
21. D. Romanini, A. A. Kachanov, N. Sadeghi, and F. Stoeckel, "CW cavity ring down spectroscopy," Chem. Phys. Lett. **264**, 316–322 (1997).
22. J. B. Paul, L. Lapson, and J. G. Anderson, "Ultrasensitive absorption spectroscopy with a high-finesse optical cavity and off-axis alignment," Appl. Opt. **40**, 4904–4910 (2001).
23. B. Ouyang and R. L. Jones, "Understanding the sensitivity of cavity-enhanced absorption spectroscopy: pathlength enhancement versus noise suppression," Appl. Phys. B **109**, 581–591 (2012).
24. A. O'Keefe, M. Gupta, T. G. Owano, and D. S. Baer, "Absorption spectroscopy instrument with increased optical cavity power without resonant frequency build-up," US patent 7,468,797 (23 December 2008).
25. R. Centeno, J. Mandon, S. M. Cristescu, and F. J. M. Harren, "Sensitivity enhancement in off-axis integrated cavity output spectroscopy," Opt. Express **22**, 27985–27991 (2014).
26. C. Dyroff, "Optimum signal-to-noise ratio in off-axis integrated cavity output spectroscopy," Opt. Lett. **36**, 1110–1112 (2011).
27. N. K. Dhar, R. Dat, and A. K. Sood, "Advances in infrared detector array technology," in *Optoelectronics—Advanced Materials*, S. L. Pyshkin and J. M. Ballato, eds. (InTech, 2013).

28. J. B. Leen and A. O'Keefe, "Optical re-injection in cavity-enhanced absorption spectroscopy," Rev. Sci. Instrum. **85**, 093101 (2014).
29. R. Centeno, J. Mandon, S. M. Cristescu, and F. J. M. Harren, "Three mirror off axis integrated cavity output spectroscopy for the detection of ethylene using a quantum cascade laser," Sens. Actuators B **203**, 311–319 (2014).
30. F. Nadeem, B. R. Postma, G. Postma, S. M. Cristescu, J. Mandon, and F. J. M. Harren, "Comprehensive three-dimensional ray tracing model for three-mirror cavity-enhanced spectroscopy," Appl. Opt. **57**, 154–163 (2018).
31. D. Herriott, H. Kogelnik, and R. Kompfner, "Off-axis paths in spherical mirror interferometers," Appl. Opt. **3**, 523–526 (1964).
32. HITRAN Database, 2018, https://www.hitran.org/.
33. M. Azhar, J. Mandon, A. H. Neerincx, Z. Liu, J. Mink, P. J. F. M. Merkus, S. M. Cristescu, and F. J. M. Harren, "A widely tunable, near-infrared laser-based trace gas sensor for hydrogen cyanide (HCN) detection in exhaled breath," Appl. Phys. B **123**, 268 (2017).
34. N. Pakmanesh, S. M. Cristescu, A. Ghorbanzadeh, F. J. M. Harren, and J. Mandon, "Quantum cascade laser-based sensors for the detection of exhaled carbon monoxide," Appl. Phys. B **122**, 10 (2016).
35. B. W. Clouser, L. Sarkozy, and E. J. Moyer, "Improved light collection in OA-ICOS cells using non-axially-symmetric optics," Appl. Opt. **57**, 6252–6259 (2018).